JOURNAL OF SANDWICH STRUCTURES & MATERIALS

Original Article

Journal of Sandwich Structures & Materials
0(0) 1–21

DOI: 10.1177/1099636218789612
journals.sagepub.com/home/jsm
SAGE

Nonlinear buckling and post-buckling analysis of imperfect porous plates under mechanical loads

Tran Minh Tu[1], Le Kha Hoa[2], Dang Xuan Hung[1] and Le Thanh Hai[3]

Abstract

The nonlinear buckling and post-buckling response of imperfect porous plates is investigated analytically in this paper. The porous materials with elastic moduli are assumed to vary through the thickness of the plate according to two different distribution types. Governing equations are derived based on the classical shell theory taking into account Von Karman nonlinearity and initial geometrical imperfection. Explicit relations of load–deflection curves for rectangular porous plates are determined by applying stress function and Galerkin's method. The accuracy of present theoretical formulation is verified by comparing it with available results in the literature. The effects of varying porosity distribution, porosity coefficient, boundary condition and imperfection on post-buckling behavior of the porous plate are studied in detail. A parametric study is carried out to investigate the effects of varying porosity distribution, porosity coefficient, boundary condition and imperfection on post-buckling behavior of the porous plate. The results show that the critical buckling loads decrease with increasing porosity coefficient and the post-buckling curves for nonlinear symmetric porosity distribution are always higher than those for nonlinear non-symmetric porosity.

Keywords

Nonlinear, buckling, post-buckling, imperfect porous plates, analytical solution

[1]Faculty of Industrial and Civil Engineering, University of Civil Engineering, Vietnam
[2]Faculty of Basic Science, Military Academy of Logistics, Hanoi 100000, Vietnam
[3]Faculty of Civil Engineering, Vinh University, Vietnam

Corresponding author:
Le Kha Hoa, Faculty of Basic Science, Military Academy of Logistics, Hanoi 100000, Vietnam.
Email: lekhahoa@gmail.com

Introduction

Fiber reinforced composites are widely used in the aerospace, automotive, marine and other structural applications. Stress singularities in such composites may occur at the interface between two different materials, due to the mismatch of materials. Functionally graded materials (FGMs) are new class of composite materials, microscopically inhomogeneous, in which the mechanical properties vary smoothly and continuously from one surface to the other. This eliminates interface problems of conventional composite material. Functionally graded (FG) porous material is a novel FGM in which porous materials are characterized by the graded distribution of internal pores in the microstructure. In the last few years, porous materials such as metal foams have been widely used for lightweight structures in aerospace, automotive and civil engineering applications because of their excellent energy-absorbing capability and low thermal and electrical conductivity [1–5].

Numerous studies on static and dynamic behaviors of composite, FG, and porous structures have been extensively carried out. Komur et al. [6] investigated buckling behavior of laminated composite plates by finite element method. Thai and Choi [7] presented efficient and simple refined theory for buckling analysis of FG plates. Magnucki and Stasiewicz [8] studied elastic buckling of porous beam; the critical load is determined analytically then verified with finite element solution. Using nonlinear hypothesis of deformation of a plane cross-section of the beam, Magnucka-Blandzi and Magnucki [9] determined the stress state and the critical force for the simply supported sandwich beam with a metal foam core.

The elastic buckling and static bending behavior of FG porous beams was investigated by Chen et al. [10] using Timoshenko beam theory. The Ritz method is employed to obtain the critical buckling loads and transverse bending deflections. The authors [11] then investigated the free and forced vibration characteristics of FG porous (open-cell metal foam) beams. Natural frequencies and transient response are examined for porous beams under different types of loading: a harmonic point load, an impulsive point load and a moving load with constant velocity.

Magnucki et al. [12] investigated the bending of simply supported porous plate loaded with transverse pressure. The critical load of a bi-axially in-plane compressed plate is found. In order to compare the analytical results, a finite element model of a porous plate is built using the ANSYS software. Rezaei and Saidi [13] developed an analytical solution based on Reddy's third-order shear deformation theory for free vibration analysis of rectangular porous plate made of Berea sandstone.

It can be seen that the majority of the above-mentioned studies are about the linear analysis of FG porous beams and plates. In engineering practice, the nonlinear behavior of these structures plays an important role. Chen et al. [14] analyzed the nonlinear free vibration behavior of sandwich porous beam based on Timoshenko beam theory. Using Kirchhoff-Love assumption taking into account the geometrical nonlinearity with Sanders non-linear strain-displacement relation,

Ebrahimi and Zia [15] investigated the large-amplitude nonlinear vibration characteristics of FG Timoshenko beams made of porous material. Jabbari et al. [16] presented buckling analysis of a radically loaded circular plate made of FG porous materials saturated with fluid. Based on higher order shear deformation plate theory, Mojahedin et al. [17] analyzed the buckling behavior of radially loaded solid circular plate made of porous material, where pores are assumed to be saturated with fluid.

As a result, there are few literature devoted to the nonlinear behavior of porous plates. Thus, the objective of this paper is to investigate the nonlinear buckling behavior of imperfect porous plates under in-plane mechanical load. The Young's moduli and mass density of porous composites (open-cell metal foam) are assumed to be graded in the thickness direction following a simple cosine rule. The mathematical formulation based on the classical plate theory and von-Karman nonlinear kinematics taking to account the initial geometrical imperfection is developed. The resulting equations are solved using Galerkin procedure to obtain closed-form expressions of the buckling loads and post-buckling load–deflection curves. The effects of material's porosity coefficient, geometric parameters and imperfection on the buckling and post-buckling behaviors of the plate are discussed in detail.

Porous plates and fundamental relations

Porous plates

Consider a thin rectangular porous plate of length a, width b and thickness h, referring to the rectangular Cartesian coordinates (x, y, z), where (x, y) plane coincides with the middle surface of the plate and z is the thickness coordinate $(-h/2 \leq z \leq h/2)$. The plate is subjected to the uniform in-plane compressive edge loads p_x and py, which are uniformly distributed along the edges $x = 0$, a and $y = 0$, b, respectively as depicted in Figure 1.

The open-cell metal foam with elasticity moduli and mass density is assumed to vary through the thickness of the plate according to two different distribution laws [10, 11].

- For the first case, pore distribution is nonlinear symmetric and the mid-plane of plate is its symmetry plane. Moduli of elasticity and mass density, which depend on pore distribution, are as follows (Porosity distribution 1)

$$\begin{aligned} E(z) &= E_1\left[1 - e_0\cos\left(\pi\frac{z}{h}\right)\right]; \quad G(z) = G_1\left[1 - e_0\cos\left(\pi\frac{z}{h}\right)\right]; \\ \rho(z) &= \rho_1\left[1 - e_m\cos\left(\pi\frac{z}{h}\right)\right] \end{aligned} \tag{1}$$

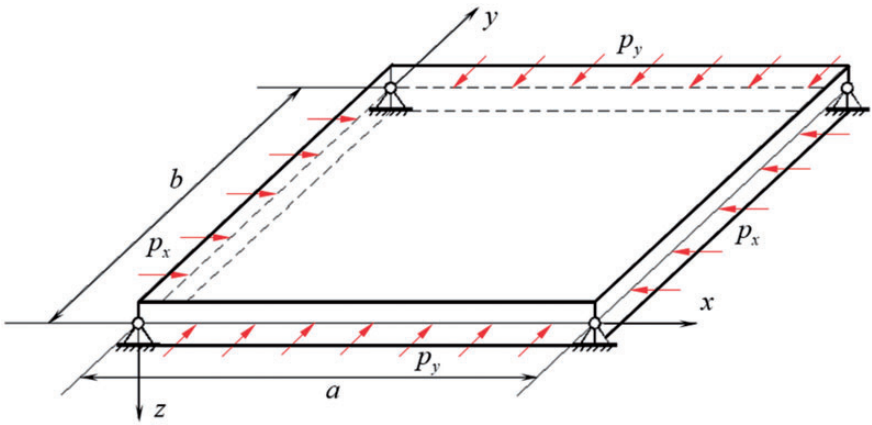

Figure 1. Rectangular porous plate under in-plane compressive loads.

where the porosity coefficient for moduli of elasticity $e_0 = 1 - \frac{E_2}{E_1} = 1 - \frac{G_2}{G_1}$; $(0<e_0<1)$ and the porosity coefficient for mass density $e_m = 1 - \frac{\rho_2}{\rho_1}$; $(0<e_m<1)$. The relationship between Young's modulus and shear modulus is $G_i = \frac{E_i}{2(1+\nu)}$ $(i = 1,2)$ where v is the Poisson's ratio and is assumed to be constant across the plate thickness; E_2, G_2, ρ_2; E_1, G_1, ρ_1 are the values of Young's moduli, shear moduli and mass density at the mid-plane $(z = 0)$ and the upper and lower surfaces of the plate $\left(z = \pm\frac{h}{2}\right)$, respectively.

The nonlinear symmetric porosity distribution is plotted in Figure 2. It can be observed that Young's moduli, shear moduli and mass density reach their maximum values at the top and bottom surfaces where the materials are pure. The minimum values are reached at the mid-surface of the plate.

- For the second case, pore distribution is nonlinear and non-symmetric. The moduli of elasticity and mass density distribution are expressed as follows (Porosity distribution 2)

$$E(z) = E_1\left[1 - e_0\cos\left(\frac{\pi}{2}\frac{z}{h} + \frac{\pi}{4}\right)\right]; \quad G(z) = G_1\left[1 - e_0\cos\left(\frac{\pi}{2}\frac{z}{h} + \frac{\pi}{4}\right)\right];$$
$$\rho(z) = \rho_1\left[1 - e_m\cos\left(\frac{\pi}{2}\frac{z}{h} + \frac{\pi}{4}\right)\right] \tag{2}$$

E_2, G_2, ρ_2; E_1, G_1, ρ_1 are the values of Young's moduli, shear moduli and mass density at the upper surface $\left(z = \frac{h}{2}\right)$ and lower surface of the plate $\left(z = -\frac{h}{2}\right)$, respectively.

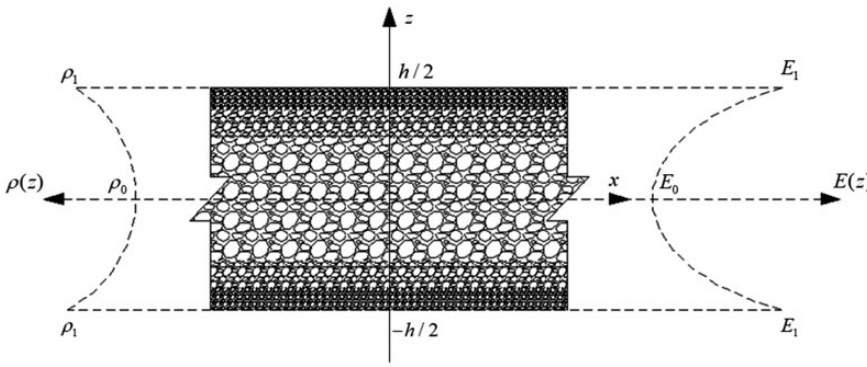

Figure 2. Nonlinear symmetric porosity distribution.

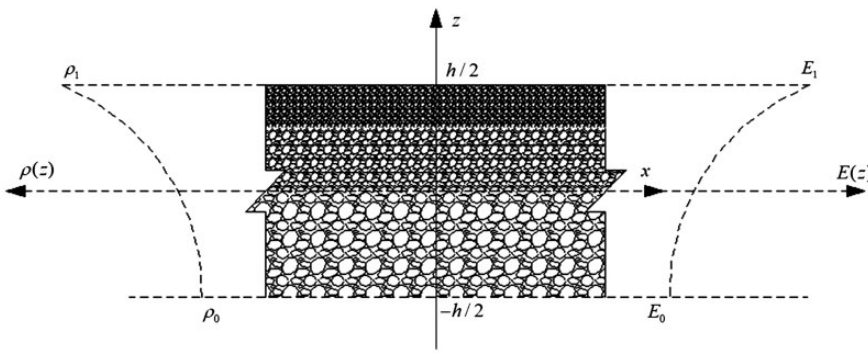

Figure 3. Nonlinear non-symmetric porosity distribution.

Figure 3 depicts the nonlinear non-symmetric porosity distribution. The plot shows that Young's moduli, shear moduli and mass density are maximum at the top surfaces, where the materials are pure, and are minimum at the bottom surface, where the porosity coefficient is the largest.

Governing relations and equations

According to the classical plate theory, the strains at the mid-plane of imperfect porous plate, taking into account geometrical nonlinearity in von Karman sense, are expressed as follows [18]

$$\begin{aligned} &\varepsilon_x^0 = u_{,x} + \frac{1}{2}w_{,x}^2 + w_{,x}w_{,x}^*; \quad \varepsilon_y^0 = \mathrm{v}_{,y} + \frac{1}{2}w_{,y}^2 + w_{,y}w_{,y}^*; \\ &\gamma_{xy}^0 = u_{,y} + \mathrm{v}_{,x} + w_{,x}.w_{,y} + w_{,x}.w_{,y}^* + w_{,y}.w_{,x}^* \end{aligned} \tag{3}$$

where $u = u(x, y)$, $\mathrm{v} = \mathrm{v}(x, y)$, $w = w(x, y)$ are the displacements of the mid-plane point along x, y and z axes, respectively. The parameter $w^* = w^*(x, y)$ is an initial imperfection of the plate and is assumed to be small compared with the thickness of the plate.

The strains at a point with coordinate z from the mid-plane are in the form [18]

$$\begin{aligned} &\varepsilon_x = \varepsilon_x^0 + zk_x;\ \varepsilon_y = \varepsilon_y^0 + zk_y;\ \gamma_{xy} = \gamma_{xy}^0 + 2zk_{xy};\\ &k_x = -w_{,xx};\ k_y = -w_{,yy};\ k_{xy} = -w_{,xy} \end{aligned} \tag{4}$$

Hooke's stress–strain relations for a plate are written as

$$(\sigma_x,\ \sigma_y) = \frac{E}{1-\nu^2}\left[(\varepsilon_x,\ \varepsilon_y) + \nu(\varepsilon_y,\ \varepsilon_x)\right];\quad \sigma_{xy} = \frac{E}{2(1+\nu)}\gamma_{xy} \tag{5}$$

The force and moment resultants per unit length of the plate are defined as

$$\left\{(N_x, N_y, N_{xy}), (M_x, M_y, M_{xy})\right\} = \int_{-h/2}^{h/2} \{\sigma_x, \sigma_y, \sigma_{xy}\}(1, z)\mathrm{d}z \tag{6}$$

Substituting equations (3), (4) and (5) into equation (6) gives the constitutive relations as

$$\begin{bmatrix} N_x \\ N_y \\ N_{xy} \\ M_x \\ M_y \\ M_{xy} \end{bmatrix} = \begin{bmatrix} A_{10} & A_{20} & 0 & A_{11} & A_{21} & 0 \\ A_{20} & A_{10} & 0 & A_{21} & A_{11} & 0 \\ 0 & 0 & A_{30} & 0 & 0 & A_{31} \\ A_{11} & A_{21} & 0 & A_{12} & A_{22} & 0 \\ A_{21} & A_{11} & 0 & A_{22} & A_{12} & 0 \\ 0 & 0 & A_{31} & 0 & 0 & A_{32} \end{bmatrix} \begin{bmatrix} \varepsilon_x^0 \\ \varepsilon_y^0 \\ \gamma_{xy}^0 \\ k_x \\ k_y \\ 2k_{xy} \end{bmatrix} \tag{7}$$

where the stiffness coefficients A_{ij} $(i = 1, 2, 3; j = 0, 1, 2)$ are defined in the forms as

$$\begin{aligned} &A_{1j} = \int_{-h/2}^{h/2} \frac{E(z)}{1-\nu^2(z)} z^j \mathrm{d}z;\quad A_{2j} = \int_{-h/2}^{h/2} \frac{E(z)\,\nu(z)}{1-\nu^2(z)} z^j \mathrm{d}z;\\ &A_{3j} = \int_{-h/2}^{h/2} \frac{E(z)}{2[1+\nu(z)]} z^j \mathrm{d}z = \frac{1}{2}(A_{1j} - A_{2j}) \end{aligned} \tag{8}$$

The nonlinear equilibrium equations of imperfect plate based on the classical plate theory are given by [19]

$$N_{x,x} + N_{xy,y} = 0 \tag{9}$$

$$N_{xy,x} + N_{y,y} = 0 \tag{10}$$

$$\begin{aligned} &M_{x,xx} + 2M_{xy,xy} + M_{y,yy} + N_x\left(w_{,xx} + w^*_{,xx}\right) + \\ &+ 2N_{xy}\left(w_{,xy} + w^*_{,xy}\right) + N_y\left(w_{,yy} + w^*_{,yy}\right) = 0 \end{aligned} \tag{11}$$

The geometrical compatibility equation obtained from equations (3) and (4), quantity $w^*_{,ij}$ is assumed to be small enough so the quadratic terms of $w^*_{,ij}$ may be neglected, becomes

$$\varepsilon^0_{x,yy} + \varepsilon^0_{y,xx} - \gamma^0_{xy,xy} = w^2_{,xy} - w_{,xx}.w_{,yy} + 2w_{,xy}w^*_{,xy} - w_{,xx}.w^*_{,yy} - w_{,yy}w^*_{,xx} \tag{12}$$

Let us introduce the stress function $f=f(x,y)$ as

$$N_x = f_{,yy}; \quad N_y = f_{,xx}; \quad N_{xy} = -f_{,xy} \tag{13}$$

It is clear that the two equations (9) and (10) are automatically satisfied.

Substitution of equation (13) into the constitutive relations for N_{ij} in equation (7) and solving conversely, we obtain

$$\begin{aligned} \varepsilon^0_x &= J_0\left(A_{10}f_{,yy} - A_{20}f_{,xx} + J_1 w_{,xx} + J_2 w_{,yy}\right) \\ \varepsilon^0_y &= J_0\left(A_{10}f_{,xx} - A_{20}f_{,yy} + J_1 w_{,yy} + J_2 w_{,xx}\right) \\ \gamma^0_{xy} &= \frac{1}{A_{30}}\left(2A_{31}w_{,xy} - f_{,xy}\right) \end{aligned} \tag{14}$$

where $J_0 = \frac{1}{A^2_{10} - A^2_{20}}$, $J_1 = A_{10}A_{11} - A_{20}A_{21}$; $J_2 = A_{10}A_{21} - A_{20}A_{11}$.

Substituting once again equation (14) into the constitutive relations of M_{ij} in equation (7), then M_{ij} into the equation (11) and taking into account equation (13), we have

$$C_3\nabla^4 f + C_4\nabla^4 w + f_{,yy}\left(w_{,xx} + w^*_{,xx}\right) - 2f_{,xy}\left(w_{,xy} + w^*_{,xy}\right) + f_{,xx}\left(w_{,yy} + w^*_{,yy}\right) = 0 \tag{15}$$

where $C_3 = J_0J_2$, $C_4 = J_0(A_{11}J_1 + A_{21}J_2) - A_{12}$.

$$\nabla^4 = \frac{\partial^4}{\partial x^4} + 2\frac{\partial^4}{\partial x^2\partial y^2} + \frac{\partial^4}{\partial y^4}$$

Equation (15) is the stability equation for an imperfect porous plate. This equation includes two unknown functions w and f. Hence it is necessary to find an additional function. For this purpose, substituting equation (14) into the compatibility equation (12), we get

$$\nabla^4 f + C_1 \nabla^4 w - C_2 \left(w_{,xy}^2 - w_{,xx} w_{,yy} + 2 w_{,xy} w_{,xy}^* - w_{,xx} w_{,yy}^* - w_{,yy} w_{,xx}^* \right) = 0 \tag{16}$$

where

$$C_1 = J_2 / A_{10},\ C_2 = 1/(J_0 A_{10})$$

The two equations (15) and (16) are the governing equations used to investigate the buckling and post-buckling behavior of imperfect porous plates. From equations (15) and (16), if $w^* = 0$, we obtain the governing equations for perfect porous plates.

Nonlinear buckling and post-buckling analysis

Boundary conditions

Two cases of boundary conditions will be considered for determining the buckling loads of porous plates under in-plane compressive load.

Case 1 (SSSS): The four edges of plate are simply supported and freely movable. The associated boundary conditions are

$$\begin{aligned} &w = M_x = N_{xy} = 0, \quad N_x = -p_x h \quad \text{at } x = 0,\ x = a \\ &w = M_y = N_{xy} = 0, \quad N_y = -p_y h \quad \text{at } y = 0,\ y = b \end{aligned} \tag{17}$$

Case 2 (SSCC): Two edges loaded $x = 0$ and $x = a$ are simply supported and freely movable, the remaining two edges $y = 0$, $y = b$ are unloaded and clamped. The associated boundary conditions are

$$\begin{aligned} &w = M_x = N_{xy} = 0, \quad N_x = -p_x h \quad \text{at } x = 0,\ x = a \\ &w = \frac{\partial w}{\partial y} = N_y = N_{xy} = 0 \quad \text{at } y = 0,\ y = b \end{aligned} \tag{18}$$

Imperfect porous plate with Case 1 of boundary condition (SSSS)

To solve equations (15) and (16), the deflection w and stress function f are assumed in the following forms [19] satisfying boundary conditions (equation (17))

$$\begin{aligned} w &= W\sin\frac{m\pi x}{a}\sin\frac{n\pi y}{b} \\ f &= F\left[\sin\frac{m\pi x}{a}\sin\frac{n\pi y}{b} - \theta(x) - \lambda(y)\right] \end{aligned} \tag{19}$$

where $m,\ n = 1,2,3,\ldots$ are the number of half-waves in x and y directions, respectively; W and F are unknown constant coefficients to be determined. Functions $\theta(x)$ and $\lambda(y)$ should be chosen such that solutions (equation (19)) satisfy the force boundary conditions, thus

$$F\frac{d^2\theta(x)}{dx^2} = p_y h, \quad F\frac{d^2\lambda(y)}{dy^2} = p_x h;$$

The initial imperfections of the plate $w^* = w^*(x, y)$ in considering the boundary conditions (equation (17)) are assumed as

$$w^* = \xi h\sin\frac{m\pi x}{a}\sin\frac{n\pi y}{b}, \quad m,\ n = 1, 2, 3, \ldots \tag{20}$$

where the coefficient $\xi \in [0,\ 1]$ expresses an imperfection size of the plate.

By substituting equations (19) and (20) into equations (15) and (16) and then applying Galerkin's procedure, we obtain two nonlinear algebraic equations for F and W in the form

$$F + C_1 W + \frac{C_2 W}{\left[\left(\frac{m\pi}{a}\right)^2 + \left(\frac{n\pi}{b}\right)^2\right]^2}\frac{16mn\pi^2}{3a^2b^2}(W + 2\xi h)\delta_1\delta_2 = 0 \tag{21}$$

$$\begin{aligned} &\left[\left(\frac{m\pi}{a}\right)^2 + \left(\frac{n\pi}{b}\right)^2\right]^2 (C_3 F + C_4 W) + \frac{32}{3}F(W + \xi h)\frac{mn\pi^2}{a^2b^2}\delta_1\delta_2 + \\ &+ (W + \xi h)\left[p_x h\left(\frac{m\pi}{a}\right)^2 + p_y h\left(\frac{n\pi}{b}\right)^2\right] = 0 \end{aligned} \tag{22}$$

Herein, note that $\delta_1 = \frac{1}{2}\left[1 - (-1)^m\right],\ \delta_2 = \frac{1}{2}\left[1 - (-1)^n\right]$, so $\delta_1\delta_2 = 1$ if m and n are odd numbers, while $\delta_1\delta_2 = 0$ if either m or n is an even number.

By eliminating F in equations (21) and (22), after some manipulation we get

$$\begin{aligned}&(C_4 - C_3C_1)\pi^4(m^2B_a^2 + n^2)^4 W - \frac{16mn\pi^2 B_a^2}{3}(m^2B_a^2 + n^2)^2 \\ &\quad \times \left[(C_2C_3 + 2C_1)W + 2(C_2C_3 + C_1)\xi h\right] W\delta_1\delta_2 \\ &\quad - \frac{512m^2n^2B_a^4}{9} C_2 W(W + \xi h)(W + 2\xi h)\delta_1^2\delta_2^2 \\ &\quad + \pi^2 b^2 p_x h(m^2B_a^2 + n^2)^2\left(m^2B_a^2 + \beta n^2\right)(W + \xi h) = 0\end{aligned} \tag{23}$$

where

$$B_a = b/a; \quad \beta = p_y/p_x$$

Equation (23) expresses the load–deflection relation, and it is used to analyze the buckling and post-buckling behaviors of imperfect porous plates subjected to in-plane loads p_x and p_y

$$\begin{aligned}p_x = &-\frac{(C_4 - C_3C_1)\pi^4(m^2B_a^2 + n^2)^2}{\pi^2 b^2 h\left(m^2B_a^2 + \beta n^2\right)}\frac{\overline{W}}{\left(\overline{W} + \xi\right)} + \\ &+ \frac{16mn\pi^2 B_a^2}{3\pi^2 b^2\left(m^2B_a^2 + \beta n^2\right)}\left[(C_2C_3 + 2C_1)\overline{W} + 2(C_2C_3 + C_1)\xi\right]\frac{\overline{W}}{\left(\overline{W} + \xi\right)}\delta_1\delta_2 + \\ &+ \frac{512m^2n^2B_a^4 h}{9(m^2B_a^2 + n^2)^2\pi^2 b^2\left(m^2B_a^2 + \beta n^2\right)} C_2\overline{W}(\overline{W} + 2\xi)\delta_1^2\delta_2^2\end{aligned} \tag{24}$$

In the case where the plate is only subjected to uni-axial compressive load, we take the pre-buckling force resultants as $N_{x0} = -p_x h$, $N_{y0} = -p_y h = 0$. From equation (24), we obtain

$$\begin{aligned}p_x = &\frac{\overline{W}}{\left(\overline{W} + \xi\right)}\frac{\pi^2(m^2B_a^2 + n^2)^2}{B_h^2 m^2 B_a^2}\left(\overline{D} + \overline{C}_3\overline{C}_1\right) + \frac{512n^2B_a^2\overline{E_1}}{9\pi^2 B_h^2(m^2B_a^2 + n^2)^2}\overline{W}(\overline{W} + 2\xi) + \\ &+ \frac{16nh}{3b^2 m}\frac{\overline{W}}{\left(\overline{W} + \xi\right)}\left[\left(\overline{E_1}h^2\overline{C_3} + 2\overline{C_1}\right)\overline{W} + 2\left(\overline{E_1}h^2\overline{C_3} + \overline{C_1}\right)\xi\right]\end{aligned} \tag{25}$$

where m, n are odd numbers, and

$$\overline{D} = -\frac{C_4}{h^3}; \quad \overline{E_1} = \frac{C_2}{h}; \quad B_h = \frac{b}{h}; \quad \overline{W} = \frac{W}{h}; \ \overline{C_1} = \frac{C_1}{h}; \quad \overline{C_3} = \frac{C_3}{h^2}.$$

For a perfect plate ($\xi = 0$) only subjected to uni-axial compressive load p_x, equation (25) leads to

$$\begin{aligned} p_x = {} & \frac{\pi^2 (m^2 B_a^2 + n^2)^2}{B_h^2 m^2 B_a^2} \left(\overline{D} + \overline{C}_3 \overline{C}_1\right) + \frac{16nh}{3b^2 m} \left(\overline{E_1} h^2 \overline{C_3} + 2\overline{C}_1\right) \overline{W} \\ & + \frac{512 n^2 B_a^2 \overline{E_1}}{9\pi^2 B_h^2 (m^2 B_a^2 + n^2)^2} \overline{W^2} \end{aligned} \tag{26}$$

So that the buckling compressive load can be determined from equation (26) by setting $W \to 0$ as

$$p_{xb} = \frac{\pi^2 (m^2 B_a^2 + n^2)^2}{B_h^2 m^2 B_a^2} \left(\overline{D} + \overline{C}_3 \overline{C}_1\right) \tag{27}$$

The buckling loads p_{xb} given by equation (27) depend on the values of m and n. By minimizing these expressions with respect to m and n, we get the critical buckling load (p_{cr}).

Imperfect porous plate with Case 2 of boundary condition (SSCC)

For this case of boundary condition, the approximate solutions satisfying boundary conditions (equation (18)) are assumed as follows [20]

$$\begin{aligned} w &= W \sin \frac{m\pi x}{a} \left(1 - \cos \frac{2n\pi y}{b}\right) \\ f &= F\left[\sin \frac{m\pi x}{a} \sin \frac{n\pi y}{b} - \lambda(y)\right], \quad F\lambda''(y) = p_x h \end{aligned} \tag{28}$$

$$w^* = \xi h \sin \frac{m\pi x}{a} \left(1 - \cos \frac{2n\pi y}{b}\right), \quad m, n = 1, 2, 3, \ldots \tag{29}$$

Similar to subsection "Imperfect porous plate with Case 1 of boundary condition (SSSS)", we substitute equation (28) and (29) into left side of equations (15)

and (16), and then using Galerkin's procedure, we obtain

$$F=\frac{1}{A}\left\{-W\frac{4C_1}{3n\pi}\delta_2\left[3\left(\frac{m\pi}{a}\right)^4+B\right]-C_2W(W+2\xi h)\frac{1024mn\pi^2}{45a^2b^2}\delta_1\delta_2\right\} \tag{30}$$

$$\begin{aligned}&C_3A\frac{4ab}{3n\pi}\delta_2F+C_4W\frac{ab}{4}\left[2\left(\frac{m\pi}{a}\right)^4+B\right]+F(W+\xi h)\left(\frac{mn\pi^2}{ab}\right)^2\frac{512ab}{45mn\pi^2}\delta_1\delta_2\\&+p_xh(W+\xi h)\left(\frac{m\pi}{a}\right)^2\frac{3ab}{4}+q\frac{2ab}{m\pi}\delta_1=0\end{aligned} \tag{31}$$

where $A=\left[\left(\frac{m\pi}{a}\right)^2+\left(\frac{n\pi}{b}\right)^2\right]^2$; $B=\left[\left(\frac{m\pi}{a}\right)^2+\left(\frac{2n\pi}{b}\right)^2\right]^2$.

Eliminating F in equations (30) and (31), we get

$$\begin{aligned}&\alpha_1\,W+\alpha_2\,W(W+2\xi h)+\alpha_3\,W(W+\xi h)+\\&+\alpha_4\,W(W+\xi h)(W+2\xi h)+p_xh(W+\xi h)\frac{3bm^2\pi^2}{4a}=0\end{aligned} \tag{32}$$

in which

$$\begin{aligned}\alpha_1&=-\frac{16abC_1C_3}{9n^2\pi^2}\delta_2^2\left[3\left(\frac{m\pi}{a}\right)^4+B\right]+\frac{abC_4}{4}\left[2\left(\frac{m\pi}{a}\right)^4+B\right],\\\alpha_2&=-\frac{4096m\pi C_2C_3}{135ab}\delta_1\delta_2^2\\\alpha_3&=-\frac{2048m\pi C_1}{135abA}\left[3\left(\frac{m\pi}{a}\right)^4+B\right]\delta_1\delta_2^2,\\\alpha_4&=-\frac{524288m^2n^2\pi^4C_2}{2025a^3b^3A}(\delta_1\delta_2)^2\end{aligned} \tag{33}$$

From equation (32), we have

$$p_x=\frac{-4a}{3bm^2\pi^2}\left[\alpha_1\frac{\overline{W}}{h\left(\overline{W}+\xi\right)}+\alpha_2\frac{\overline{W}(\overline{W}+2\xi)}{\left(\overline{W}+\xi\right)}+\alpha_3\overline{W}+\alpha_4h\,\overline{W}(\overline{W}+2\xi)\right] \tag{34}$$

Herein, we denote $\overline{W}=W/h$.

If a plate is perfect ($\xi = 0$), equation (38) becomes

$$p_x = \frac{-4a}{3bm^2\pi^2}\left[\frac{\alpha_1}{h} + (\alpha_2 + \alpha_3)\,\overline{W} + \alpha_4 h\,\overline{W}^2\right] \tag{35}$$

From this relationship, let $\overline{W} \to 0$, we obtain the expression of buckling compressive load as

$$p_{xb} = \frac{-4a}{3bm^2\pi^2 h}\,\alpha_1 = \frac{64a^2C_1C_3}{27m^2n^2\pi^4 h}\,\delta_2^2\left[3\left(\frac{m\pi}{a}\right)^4 + B\right] - \frac{a^2C_4}{3m^2\pi^2 h}\left[2\left(\frac{m\pi}{a}\right)^4 + B\right] \tag{36}$$

Buckling loads p_{xb} given by equation (36) depend on the values of m and n; by minimizing these expressions with respect to m and n we get the critical buckling load (p_{cr}).

Numerical calculations and discussions

Validation examples

The first validation is carried out for simply supported isotropic rectangular plate under uniaxial in-plane compression. Table 1 shows the comparisons of the critical buckling loads with the results given in the monograph of Brush and Almroth [18], in which the analytical formulae of critical load is given. The input parameters are $e_0 = 0$, $h = 0.1$ in., $b = 10$ in, $a = 20$ in., $P_x = p_x bh$ where p_x is found from equation (27).

For the second validation, the post-buckling load–deflection curves of isotropic square plate ($e_0 = 0$) are plotted for perfect and imperfect cases with the following geometric and material properties: $E_1 = 380\,\text{GPa}$; $\nu_1 = 0.3$; $b/h = 40$; $a/b = 1$. Figure 4 shows the comparison of the present post-buckling load–deflection curves of isotropic plate ($e_0 = 0$) with those of Tung and Duc [19].

As can be seen, a good agreement is obtained in the two above-mentioned comparisons.

Parametric study

Parametric studies are performed to investigate the effects of the porosity coefficient, the imperfection and geometrical parameters on the buckling load of porous plates. The considered porous plates are assumed to be composed of the open-cell steel foam with $E_1 = 207\,\text{GPa}$ and $\nu_1 = 0.3$.

Table 1. Critical buckling load for isotropic plate under uniaxial in-plane compression.

P_{cr} [pound]	Present $P_x = p_{upper}bh$	Brush and Almroth [18] $P_x = \left(\frac{mb}{a} + \frac{a}{mb}\right)^2 \frac{\pi^2 D}{b}$; $D = \frac{Eh^3}{12(1-\nu^2)}$
$E = 10 \times 10^6$psi, $v = 0.3$ Aluminum (Al)	3615.2397 (2, 1)[a]	3620 (2, 1)
$E = 15.1 \times 10^6$ psi, $v = 0.3$ Titanium alloy (Ti-6Al-4V)	5459.0120 (2, 1)	5459 (2, 1)
$E = 30.1 \times 10^6$ psi, $v = 0.3$ Stainless steel (SUS 304)	10881.8715 (2, 1)	10882 (2, 1)

[a]The numbers in the parenthesis denote the buckling modes (m, n).

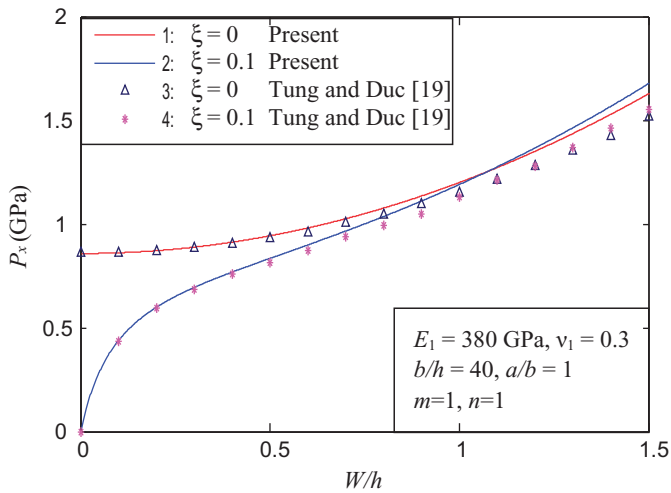

Figure 4. Post-buckling load–deflection curves of isotropic square plate.

Two cases of boundary condition and two different porosity distributions are considered:

- SSSS: All four edges of plate are simply supported
- SSCC: Two edges are simply supported and two edges are clamped
- D1: Porosity distribution 1 – equation (1)
- D2: Porosity distribution 2 – equation (2)

Table 2 presents the critical buckling loads of perfect ($\xi = 0$) rectangular (h = 2 mm; b/h = 30; a/b = 2) porous plates for various values of porosity coefficients corresponding to the buckling mode (m, n). Figure 5 illustrates the effect of porosity coefficient on the critical buckling loads of rectangular porous plates for

Table 2. Critical buckling loads of perfect rectangular of porous plates with different values of porosity coefficients of two types of porosity distribution, and various boundary conditions.

	Porosity distribution 1 – D1		Porosity distribution 2 – D2	
P_{cr} (MPa)	SSSS	SSCC	SSSS	SSCC
$e_0 = 0$	831.5051 (2, 1)[a]	1514.8022 (3, 1)	831.5051 (2, 1)	1514.8022 (3, 1)
$e_0 = 0.2$	771.3398 (2, 1)	1405.1954 (3, 1)	731.4276 (2, 1)	1332.4850 (3, 1)
$e_0 = 0.4$	711.1745 (2, 1)	1295.5887 (3, 1)	622.0666 (2, 1)	1133.2556 (3, 1)
$e_0 = 0.6$	651.0092 (2, 1)	1185.9819 (3, 1)	497.6846 (2, 1)	906.6615 (3, 1)
$e_0 = 0.8$	590.8438 (2, 1)	1076.3752 (3, 1)	346.5888 (2, 1)	631.4014 (3, 1)

[a]The numbers in the parenthesis denote the buckling modes (m, n).

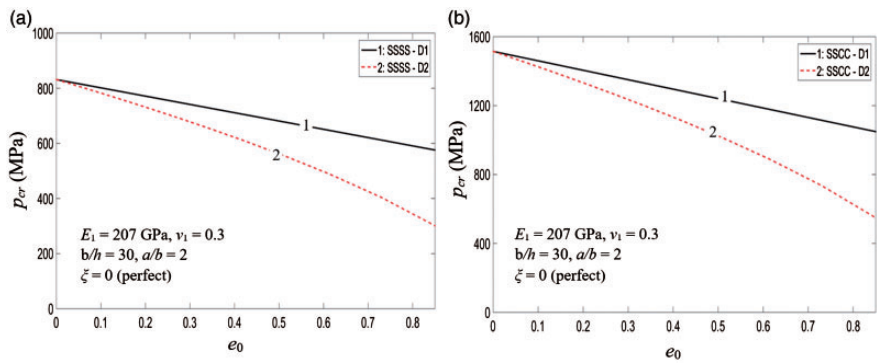

Figure 5. Effects of porosity coefficient e_0 on buckling loads P_{cr}. (a) For SSSS porous plates. (b) For SSCC porous plates.

different boundary condition (BCs) (SSSS and SSCC) and porosity distributions (D1 and D2). For both distributions, it is found that the critical buckling loads p_{cr} of porous plates decrease with increasing e_0. Figure 5 also indicates that varying porosity coefficient has a more significant effect on the stiffness of the porous plates with porosity distribution 2 (D2).

Figures 6 and 7 show post-buckling curves of perfect $(\xi = 0)$ and imperfect $(\xi = 0.2)$ rectangular $(a/b = 2)$ porous ($e_0 = 0$; 0.2; 0.4; 0.6) plates under uniaxial compression with two different porosity distributions (D1 and D2) for two cases of BC: (a) SSSS and (b) SSCC corresponding to the buckling mode with $(m = 3; n = 1)$. As can be seen, the postbuckling curves for lower porosity coefficient are always higher than those for higher porosity coefficient. It is also evident that the post-buckling curves under the SSCC boundary condition are always higher than those under the SSSS boundary condition.

Figure 8 illustrates the post-buckling curves of perfect $(\xi = 0)$ and imperfect $(\xi = 0.2)$ rectangular $(a/b = 2)$ porous $(e_0 = 0.2)$ plates under uniaxial

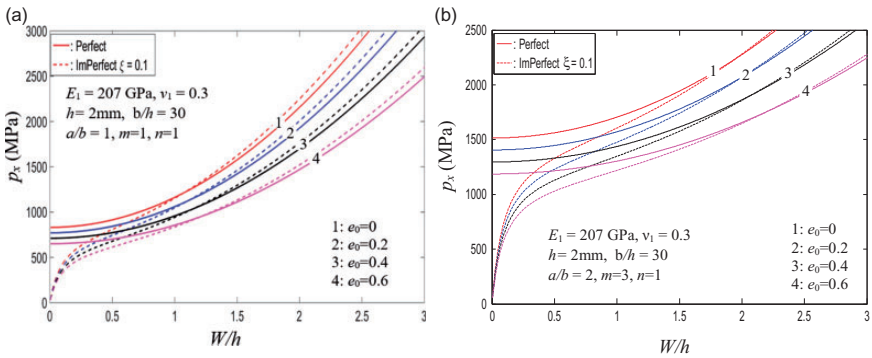

Figure 6. Effects of porosity coefficient e_0 on post-buckling load–deflection curves (D1). (a) For SSSS porous plates. (b) For SSCC plates.

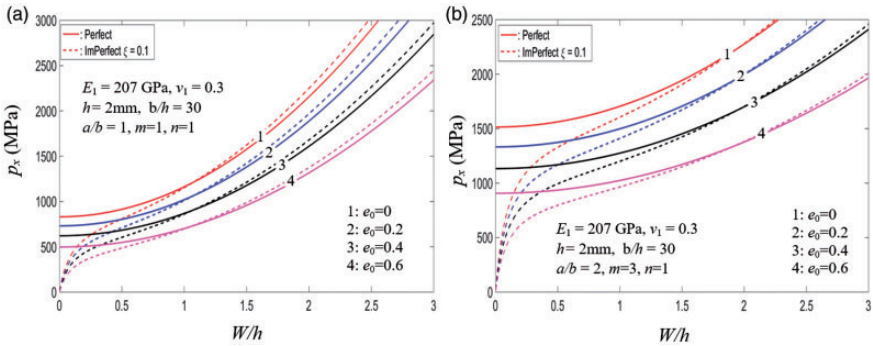

Figure 7. Effects of porosity coefficient e_0 on post-buckling load–deflection curves (D2). (a) For simply SSSS plates. (b) For SSCC plates.

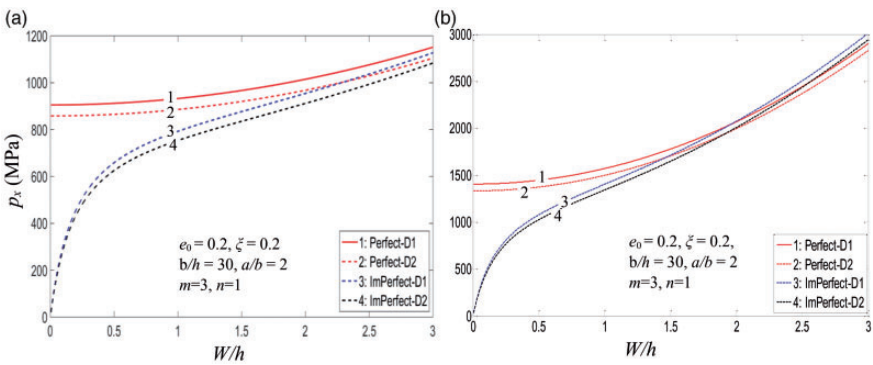

Figure 8. Effects of imperfection ξ on post-buckling load–deflection curves. (a) For SSSS porous plates. (b) For SSCC porous plates.

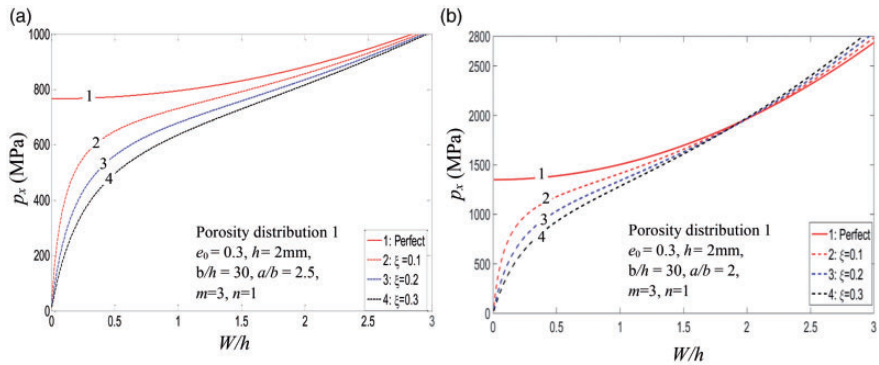

Figure 9. Effects of imperfection ξ on post-buckling load–deflection curves (D1). (a) For SSSS porous plates. (b) For SSCC plates.

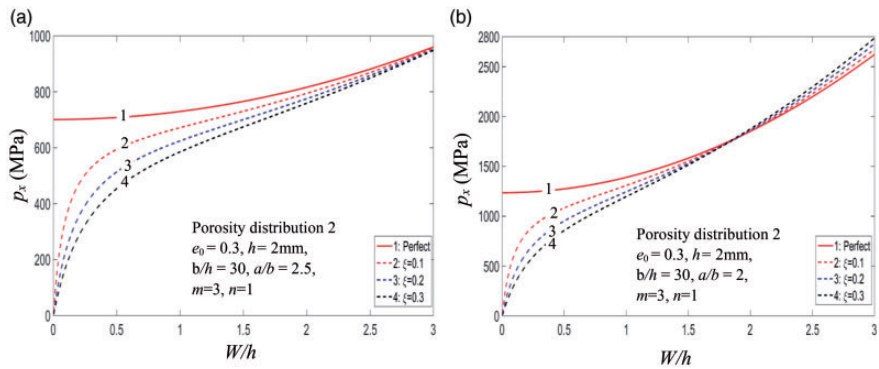

Figure 10. Effects of imperfection ξ on post-buckling load–deflection curves (D2). (a) For SSSS porous plates. (b) For SSCC porous plates.

compression with two different porosity distributions (D1 and D2) for two cases of BC: (a) SSSS and (b) SSCC corresponding to $(m = 3; n = 1)$. It is observed that the postbuckling curves for D1 porosity distribution are always higher than those for D2 porosity distribution. The effect of imperfection parameter on the post-buckling behavior of porous plates under uniaxial compression is illustrated in Figures 9 and 10. It is clear that the post-buckling curves of imperfect plates are lower than those of perfect plates when deflection is small as expected.

It is also shown that the post-buckling curves become lower as ξ increases. It means, initial imperfection makes porous plates more stable under uniaxial compression.

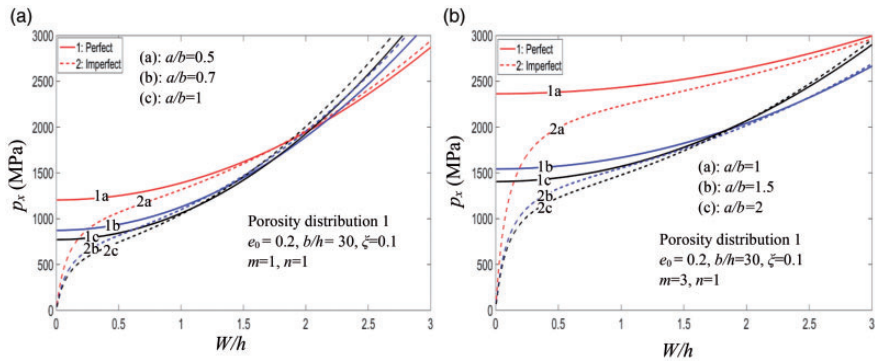

Figure 11. Effects of ratio *a/b* on post-buckling load–deflection curves. (a) For SSSS porous plates. (b) For SSCC porous plates.

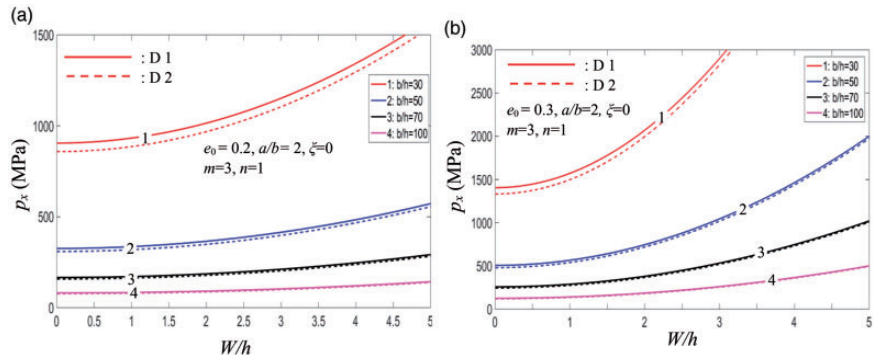

Figure 12. Effects of ratio *b/h* on post-buckling load–deflection curves. (a) For SSSS porous plates. (b) For SSCC porous plates.

Figure 11 depicts the $(p_x - W/h)$ post-buckling curves versus the aspect ratio a/b. It is shown that the buckling load decreases remarkably with increasing aspect ratio.

Figures 12 and 13 illustrate the effect of thickness-to-side ratio on the post-buckling load–deflection curves for porous plate for both porosity distributions and for two different boundary conditions. As can be observed, the buckling loads decrease significantly with increasing thickness-to-side ratios.

Figure 13 also shows the effect of boundary conditions on the post-buckling of porous plates under uniaxial compressive loads. The post-buckling load–deflection curve in the case of SSCC boundary condition is always higher than in the case of SSSS boundary condition. In addition, with certain boundary condition, the buckling loads for porosity distribution D1 are always higher than for porosity distribution D2.

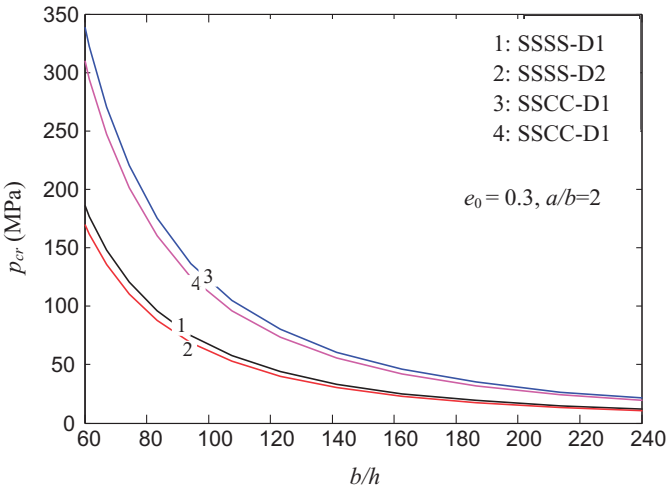

Figure 13. Effects of ratio *b/h* on post-buckling load–deflection curves.

Conclusions

This paper presents an analytical approach to study buckling and post-buckling response of thin porous plates under in-plane edge compressive loads. Theoretical formulations are within the framework of classical plate theory with both geometrical nonlinearity in von Karman sense and initial imperfection.

Galerkin's method is employed to obtain the closed-form expressions of post-buckling load–deflection curves of a porous plate with two types of porosity distribution. The effects of porosity coefficient, imperfection and geometric parameters of porous plates are investigated. The results show that post-buckling behavior of porous plates is significantly influenced by porosity coefficient, porosity distribution, imperfection, geometric parameters and in-plane boundary conditions. Furthermore, a few conclusions can be summarized from the numerical results:

1. The critical buckling loads decrease and the porous plate will be unstable by increasing porosity coefficient. Therefore, porosity distribution has a major role on the buckling behavior and should be considered in stability analysis of porous plates.
2. The post-buckling curves for nonlinear symmetric porosity distribution are higher than those for nonlinear asymmetric porosity distribution. This indicates that the FGM plates with symmetrically distributed porosity can achieve the higher stiffness hence the better mechanical performance.
3. The buckling load decreases remarkably with increasing aspect ratio and thickness-to-side ratios.

4. The post-buckling curves of imperfect plates are lower than those of perfect plates. It is evident that the perfect plate has a better mechanical loading capacity than those of the imperfect plate.

Finally, it is concluded that the analysis and thereafter results presented in this paper would be very useful for engineering design of such structures.

Highlights

- Analytical approach to investigate the nonlinear buckling and post-buckling behavior of imperfect porous plates under in-plane edge compressive loads.
- Galerkin's method is employed to obtain the closed-form expressions of post-buckling load–deflection curves of a porous plate with two types of porosity distribution.
- The effects of porosity coefficient, imperfection and geometric parameters of porous plates are investigated. The results show that post-buckling behavior of porous plates is significantly influenced by porosity coefficient, porosity distribution, imperfection, geometric parameters and in-plane boundary conditions.

Authors' Note

Le Kha Hoa is now affiliated to Faculty of Basic Science, Military Academy of Logistics, Hanoi, Vietnam.

Declaration of conflicting interests

The author(s) declared no potential conflicts of interest with respect to the research, authorship, and/or publication of this article.

Funding

The author(s) disclosed receipt of the following financial support for the research, authorship, and/or publication of this article: This work was supported by the Foundation for Science and Technology Development of National University of Civil Engineering – Ha Noi – Vietnam (Project code 213-2018/KHXD-TD).

ORCID iD

Tran Minh Tu http://orcid.org/0000-0002-2208-3463
Le Kha Hoa http://orcid.org/0000-0001-6558-3313

References

1. Smith BH, Szyniszewski S, Hajjar JF, et al. Steel foam for structures: a review of applications, manufacturing and material properties. *J Constr Steel Res* 2012; 71: 1–10.
2. Ashby M, Evans A, Fleck N, et al. *Metal foams: a design guide*. *Applied Mechanics Reviews* 2001; 54: B105.

3. Banhart J. Manufacture, characterisation and application of cellular metals and metal foams. *Progr Mater Sci* 2001; 46: 559–632.
4. Lefebvre LP, Banhart J and Dunand DC. Porous metals and metallic foams: current status and recent developments. *Adv Eng Mater* 2008; 10: 775–787.
5. Dukhan N. *Metal foams: fundamentals and applications*. Pennsylvania: DEStech Publications, Inc, 2013.
6. Komur MA, Sen F, Atas A, et al. Buckling analysis of laminated composite plates with an elliptical/circular cutout using FEM. *Adv Eng Software* 2010; 41: 161–164.
7. Thai HT and Choi DH. An efficient and simple refined theory for buckling analysis of functionally graded plates. *Appl Math Modell* 2012; 36: 1008–1022.
8. Magnucki K and Stasiewicz P. Elastic buckling of a porous beam. *J Theoretical Appl Mech* 2004; 42: 4859–4868.
9. Magnucka-Blandzi E and Magnucki K. Effective design of a sandwich beam with a metal foam core. *Thin-Walled Struct* 2007; 45: 432–438.
10. Chen D, Yang J and Kitipornchai S. Elastic buckling and static bending of shear deformable functionally graded porous beam. *Compos Struct* 2015; 133: 54–61.
11. Chen D, Yang J and Kitipornchai S. Free and forced vibrations of shear deformable functionally graded porous beams. *Int J Mech Sci* 2016; 108: 14–22.
12. Magnucki K, Malinowski M and Kasprzak J. Bending and buckling of a rectangular porous plate. *Steel Compos Struct* 2006; 6: 319–333.
13. Rezaei A and Saidi A. Exact solution for free vibration of thick rectangular plates made of porous materials. *Compos Struct* 2015; 134: 1051–1060.
14. Chen D, Kitipornchai S and Yang J. Nonlinear free vibration of shear deformable sandwich beam with a functionally graded porous core. *Thin-Walled Struct* 2016; 107: 39–48.
15. Ebrahimi F and Zia M. Large amplitude nonlinear vibration analysis of functionally graded Timoshenko beams with porosities. *Acta Astronautica* 2015; 116: 117–125.
16. Jabbari M, Mojahedin A, Khorshidvand AR, et al. Buckling analysis of a functionally graded thin circular plate made of saturated porous materials. *J Eng Mech* 2013; 140: 287–295.
17. Mojahedin A, Jabbari M, Khorshidvand AR, et al. Buckling analysis of functionally graded circular plates made of saturated porous materials based on higher order shear deformation theory. *Thin-Walled Struct* 2016; 99: 83–90.
18. Brush DO and Almroth BO. *Buckling of bars, plates, and shells*. New York: Mc Graw-Hill, 1975.
19. Tung HV and Duc ND. Nonlinear analysis of stability for functionally graded plates under mechanical and thermal loads. *Compos Struct* 2010; 92: 1184–1191.
20. Volmir AS. *Non-linear dynamics of plates and shells*. Science Edition, Moscow (1972) [in Russian]